Plasma Chemistry and Plasma Processing, Vol. 9, No. 1, 1989

Two-Dimensional Electromagnetic Field Effects in Induction Plasma Modelling

Javad Mostaghimi[1] and Maher I. Boulos[1]

Received May 26, 1987; revised April 3, 1988

Based on the electromagnetic vector potential representation, a two-dimensional, axisymmetric model is proposed for the calculation of the electromagnetic fields in an inductively coupled, radiofrequency (r.f.) plasma. A comparative analysis made between the flow, temperature, and electromagnetic fields obtained using this model and those given by our earlier one-dimensional electromagnetic fields model show relatively little difference between the temperature fields predicted by the two models. Significant differences are observed, however, between the corresponding flow and electromagnetic fields. The new model offers an effective means of accounting for variations in the coil geometry on the flow and temperature fields in the discharge and for achieving a better representation of the electromagnetic fields under higher frequency conditions (f > 10 MHz).

KEY WORDS: Modelling; induction plasmas; flow and temperature field; two-dimensional electromagnetic fields.

1. INTRODUCTION

Over the past few years there has been a renewal of interest in the inductively coupled r.f. plasma. The processing of high-purity materials, and the synthesis of ultrafine powders of metals, alloys, and ceramics are only a few examples of current and potential industrial applications of induction plasma technology. The success of these applications, however, depends to a large extent on our understanding of the basic phenomena involved and on the ability to control the conditions in the discharge.

Mathematical modelling is an excellent tool which has so far been used with considerable success to calculate the flow, temperature, and concentration fields in induction plasmas over a wide range of operating conditions.[1,2]

[1] Department of Chemical Engineering, University of Sherbrooke, Sherbrooke, Québec, J1K 2R1, Canada.

0272-4324/89/0300-0025$06.00/0

Of considerable interest are the use of these models for the development of new designs of the radiofrequency plasma torch,[3] the prediction of plasma–particle interactions under dense loading conditions,[4,5] the calculation of the emission patterns in spectrochemical ICP's,[6] and the investigation of local thermodynamic equilibrium (LTE) effects under atmospheric and reduced pressure conditions.[7] Reviews of developments in this area up to 1985 have been published by Boulos[8] and Boulos and Barnes.[9]

These studies, while being concerned with the calculation of the two-dimensional flow, temperature, and concentration fields in the discharge, were limited to a one-dimensional representation of the electromagnetic fields. The magnetic field intensity along the axis of the coil was either taken as constant, or varied according to that for a short coil in vacuum. Only the axial components of the magnetic field were considered in either case.

The assumption of one-dimensional electromagnetic fields is justified, however, only when the coil end effects are negligible. Physically, this is possible when the aspect ratio of the coil (length/diameter) is greater than unity, and for low induction frequencies.[10] Recently, based on the concept of the electromagnetic vector potential,[11,12] McKelliget[13,14] and later Mostaghimi[15] proposed a two-dimensional formulation of the electromagnetic fields in an inductively coupled plasma. The concept of electromagnetic potential is widely used in classical electrodynamics and theory of radiation. Its application to r.f. plasmas, however, is a new development which could have a long-range impact on our ability to optimize the design of an induction plasma torch both from the aerodynamic and the electromagnetic points of view. It also offers a relatively simple means of testing different induction coil designs and to determine the effect of the particular coil geometry on the flow and temperature fields in the discharge.

In this paper a two-dimensional model for the electromagnetic fields in an r.f. plasma is described. Computations are carried out for an induction plasma torch of standard design under typical operating conditions. Results are compared with those obtained using our earlier model[1,2] based on a one-dimensional representation of the electromagnetic fields.

2. THE MODEL

The proposed model is an extension of the work by Mostaghimi, Proulx, and Boulos.[1-2] The plasma is assumed to be in LTE, and optically thin. The flow is steady, laminar with negligible viscous dissipation. The flow, temperature, and electromagnetic fields are assumed to be two-dimensional with negligible displacement currents.

2.1. Vector Potential Formulation

The electromagnetic fields in the coil region of the induction plasma are governed by the Maxwell equations, which can be written in their general form as follows:

$$\nabla \cdot \mathbf{E} = 0 \tag{1}$$

$$\nabla \cdot \mathbf{H} = 0 \tag{2}$$

$$\nabla \times \mathbf{E} = -\mu_0 \frac{\partial \mathbf{H}}{\partial t} \tag{3}$$

$$\nabla \times \mathbf{H} = \mathbf{j} \tag{4}$$

with

$$\mathbf{j} = \sigma \mathbf{E} \tag{5}$$

where **E** and **H** are the electric and magnetic field intensities, respectively, **j** is the current density, μ_0 is the permeability of the free space ($\mu_0 = 4\pi \times 10^{-7}$ H/m), and σ is the electrical conductivity.

Equation (2) is satisfied through the definition of the vector potential **A** as

$$\mu_0 \mathbf{H} = \nabla \times \mathbf{A} \tag{6}$$

Substitution of Eq. (6) into Eq. (3), and considering that in the absence of an electrostatic charge on the plasma the scalar potential is equal to zero, gives the following equation for the electric field intensity as a function of the vector potential:

$$\mathbf{E} = -\frac{\partial \mathbf{A}}{\partial t} \tag{7}$$

Substituting Eq. (7) into Eq. (4) and using the identity $\nabla \times (\nabla \times \mathbf{A}) = \nabla(\nabla \cdot \mathbf{A}) - \nabla^2 \mathbf{A}$ and the Coulomb's gauge gives the following equation for the vector potential (11):

$$\nabla^2 \mathbf{A} = \mu_0 \sigma \frac{\partial \mathbf{A}}{\partial t} \tag{8}$$

Maxwell's equations are now combined into a single equation which has the following solution:

$$\mathbf{A} = \frac{\mu_0}{4\pi} \int_{v'} \frac{\mathbf{j}(\mathbf{r}', t)}{|\mathbf{r} - \mathbf{r}'|} dv' \tag{9}$$

where dv' is the volume element.

Assuming that the **A**, **E**, and **H** fields in the r.f. plasma are sinusoidal with a frequency f, they can be expressed in the time domain as follows:

$$\begin{aligned} \mathbf{A}(\mathbf{r}, t) &= \mathbf{A}_c(\mathbf{r})\, e^{i\omega t} \\ \mathbf{E}(\mathbf{r}, t) &= \mathbf{E}_c(\mathbf{r})\, e^{i\omega t} \\ \mathbf{H}(\mathbf{r}, t) &= \mathbf{H}_c(\mathbf{r})\, e^{i\omega t} \end{aligned} \tag{10}$$

where the subscript c denotes a phasor and $\omega = 2\pi f$. Substituting Eq. (10) into Eqs. (6)-(8) gives

$$\nabla^2 \mathbf{A}_c - i\mu_0 \sigma \omega \mathbf{A}_c = 0 \tag{11}$$

$$\mu_0 \mathbf{H}_c = \nabla \times \mathbf{A}_c \tag{12}$$

$$\mathbf{E}_c = -i\omega \mathbf{A}_c \tag{13}$$

For a standard induction plasma torch with a coil geometry given in Fig. 1, it is reasonable to assume that the electric field, and thus the vector potential, has only a tangential component, i.e.

$$\mathbf{A}_c = (0, A_\theta, 0) \tag{14}$$

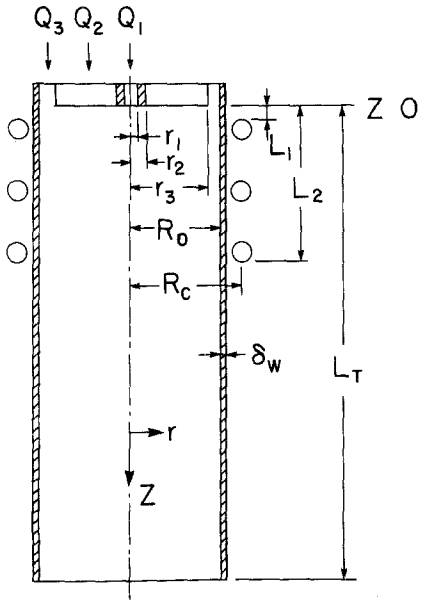

Fig. 1. Schematic diagram of the induction plasma torch.

where A_θ is also a phasor quantity. Therefore

$$\frac{1}{r}\frac{\partial}{\partial r}\left(r\frac{\partial A_\theta}{\partial r}\right)+\frac{\partial^2 A_\theta}{\partial z^2}-\left(i\mu_0\sigma\omega+\frac{1}{r^2}\right)A_\theta=0 \tag{15}$$

and

$$E_\theta=-i\omega A_\theta \tag{16}$$

$$\mu_0 H_z=\frac{1}{r}\frac{\partial}{\partial r}(rA_\theta) \tag{17}$$

$$\mu_0 H_r=-\frac{\partial}{\partial z}(A_\theta) \tag{18}$$

The boundary condition for Eq. (15) is given as

$$A_\theta(0, z)=0 \tag{19}$$

Using Eq. (9), the boundary conditions on the wall will be evaluated in the following manner.

Consider a cylindrical loop of radius R_c, carrying a current I, as shown in Fig. 2. The right-hand side of Eq. (9) can be integrated and the result is[12]

$$A_\theta(r, z)=\frac{\mu_0 I}{2\pi}\sqrt{\frac{R_c}{r}}\,G(k) \tag{20}$$

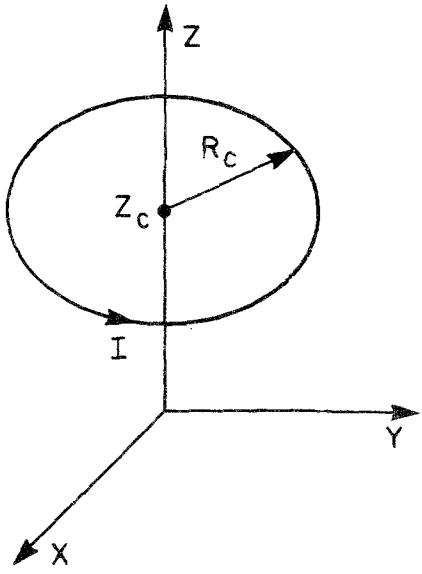

Fig. 2. Schematic representation of a current loop of the induction coil.

where

$$G(k)=\frac{(2-k^2)K(k)-2E(k)}{k} \tag{21}$$

$$k^2=\frac{4R_c r}{(R_c+r)+(z-z_c)^2} \tag{22}$$

K and E are the complete elliptic integrals.[15,16]

This result can be used to develop an expression for the wall boundary conditions. According to Eq. (9), the vector potential at each point depends on all the current-carrying regions of space. Therefore the vector potential on the wall is determined by the superposition of the coil and the plasma effects. Since, in our numerical scheme, the plasma torch will be divided into a number of control volumes in the form of cylindrical loops,[1] the wall boundary conditions can be written as

$$A_\theta(R_0, z)=\frac{\mu_0 I}{2\pi}\sqrt{\frac{R_c}{R_0}}\sum_{i=1}^{\text{coil}} G(k_i)+\frac{\mu_0}{2\pi}\sum_{i=1}^{\text{C.V.}}\sqrt{\frac{r_i}{R_0}}j_i S_i G(k_i) \tag{23}$$

where the first summation extends over the number of coils and the second one extends over the current carrying regions of the discharge. Here j_i is the current density of the ith control volume, R_0 is the radius of the plasma confinement tube, and r_i and S_i are the radius and cross section of the ith control volume.

The boundary condition for the inlet of the torch may also be determined in the same fashion. However, this condition does not have a significant effect on the solution obtained since the electrical conductivity in the inlet region is equal to zero. At the exit of the torch, on the other hand, the intensity of the magnetic and electric fields gradually drops to zero with the increase of the distance from the downstream end of the induction coil. Simpler conditions will, therefore, be adopted for the inlet and the exit regions of the torch.

For the purpose of the numerical solution of Eq. (15) with the boundary conditions, Eqs. (19) and (23), the vector potential must be divided into its components, i.e.

$$A_\theta = A_R + iA_I \tag{24}$$

where A_R and A_I are, respectively, its real and imaginary parts, and $i=\sqrt{-1}$. The individual equations and the boundary conditions for these components are given in the next section along with the governing equations for the conservation of mass, momentum, and energy.

2.2. Governing Equations

These equations are as follows:

Continuity:

$$\frac{\partial(\rho u)}{\partial z}+\frac{1}{r}\frac{\partial(\rho r v)}{\partial r}=0 \tag{25}$$

Momentum:

$$\rho u\frac{\partial u}{\partial z}+\rho v\frac{\partial u}{\partial r}=-\frac{\partial p}{\partial z}+2\frac{\partial}{\partial z}\left(\mu\frac{\partial u}{\partial z}\right)+\frac{1}{r}\frac{\partial}{\partial r}\left[\mu r\left(\frac{\partial u}{\partial r}+\frac{\partial v}{\partial z}\right)\right]+F_z \tag{26}$$

$$\rho\mu\frac{\partial v}{\partial z}+\rho v\frac{\partial v}{\partial r}=-\frac{\partial p}{\partial r}+\frac{\partial}{\partial z}\left[\mu\left(\frac{\partial v}{\partial z}+\frac{\partial u}{\partial r}\right)\right]+\frac{2}{r}\frac{\partial}{\partial r}\left[\mu r\left(\frac{\partial v}{\partial r}\right)\right]+F_r \tag{27}$$

Energy:

$$\rho u\frac{\partial h}{\partial z}+\rho v\frac{\partial h}{\partial r}=\frac{\partial}{\partial z}\left(\frac{\lambda}{c_p}\frac{\partial h}{\partial z}\right)+\frac{1}{r}\frac{\partial}{\partial r}\left(\frac{\lambda}{c_p}r\frac{\partial h}{\partial r}\right)+P-\dot{R} \tag{28}$$

Vector potential:

$$\frac{\partial^2 A_R}{\partial z^2}+\frac{1}{r}\frac{\partial}{\partial r}\left(r\frac{\partial A_R}{\partial r}\right)-\frac{A_R}{r^2}+\mu_0\sigma\omega A_I=0 \tag{29}$$

$$\frac{\partial^2 A_I}{\partial z^2}+\frac{1}{r}\frac{\partial}{\partial r}\left(r\frac{\partial A_I}{\partial r}\right)-\frac{A_I}{r^2}-\mu_0\sigma\omega A_R=0 \tag{30}$$

where u and v are, respectively, the axial and the radial velocity components; ρ, μ, λ, and c_p are the density, viscosity, thermal conductivity, and specific heat at constant pressure, respectively; h is the enthalpy, p is pressure, and P and $\dot{R}$ are the local energy dissipation rate and volumetric radiation heat losses.

$$F_r=\tfrac{1}{2}\mu_0\,\text{Real}\,[E_\theta H_z^*] \tag{31}$$

$$F_z=-\tfrac{1}{2}\mu_0\sigma\,\text{Real}\,[E_\theta H_r^*] \tag{32}$$

$$P=\tfrac{1}{2}\sigma[E_\theta E_\theta^*] \tag{33}$$

the superscript * denotes the complex conjugate. The boundary conditions for the conservation equations are:

Inlet conditions ($z=0$):

$$u=\begin{cases}Q_1/\pi r_1^2 & r<r_1\\ 0 & r_1\le r\le r_2\\ Q_2/\pi(r_3^2-r_2^2) & r_2<r\le r_3\\ Q_3/\pi(R_0^2-r_3^2) & r_3<r\le R_0\end{cases}$$

$$v = 0 \tag{34}$$

$$T = T_i$$

$$\frac{\partial^2 A_R}{\partial z^2} = \frac{\partial^2 A_I}{\partial z^2} = 0$$

Centerline $(r = 0)$:

$$\frac{\partial u}{\partial r} = v = \frac{\partial h}{\partial r} = A_R = A_I = 0 \tag{35}$$

Wall $(r = R_0)$:

$$u = v = 0$$

$$\lambda \frac{\partial T}{\partial r} = \frac{\lambda_w}{\delta_w}(T_s - T_w)$$

$$A_R = \frac{\mu_0 I}{2\pi}\sqrt{\frac{R_c}{R_0}}\sum_{i=1}^{\text{coil}} G(k_i) + \frac{\mu_0 \omega}{2\pi}\sum_{i=1}^{\text{C.V.}}\sqrt{\frac{r_i}{R_0}}\,\sigma_i A_{I,i} S_i G(k_i) \tag{36}$$

$$A_I = -\frac{\mu_0 \omega}{2\pi}\sum_{i=1}^{\text{C.V.}}\sqrt{\frac{r_i}{R_0}}\,\sigma_i A_{R,i} S_i G(k_i)$$

where λ_w is the thermal conductivity of the quartz plasma confinement tube ($\lambda_w = 1.047$ W/mK) and δ_w is the tube wall thickness. T_s and T_w are respectively, the inside and external surface temperature of the quartz tube. Since the real part of the vector potential at the wall is dominated by the coil current, the second term for this boundary condition can be neglected.

In Eq. (36), for the vector potential boundary condition, either the coil current I or the total power dissipated into the discharge P_0 can be specified. The latter is defined as

$$P_0 = \int_{v'} P(v')\, dv' \tag{37}$$

where $P(v')$ is local energy dissipation rate, Eq. (33).

Exit $(z = L_T)$:

$$\frac{\partial(\rho u)}{\partial z} = \frac{\partial v}{\partial z} = \frac{\partial h}{\partial z} = \frac{\partial^2 A_R}{\partial z^2} = \frac{\partial^2 A_I}{\partial z^2} = 0 \tag{38}$$

2.3. Thermodynamic and Transport Properties

The density, thermal conductivity, enthalpy, and viscosity data for atmospheric argon are obtained from Ref. 17. The radiation properties used here are those of Ref. 18, and the electrical conductivity is from 19.

3. RESULTS AND DISCUSSION

In this section the proposed formulation of the vector potential model is first tested and validated against exact standard solutions for the relatively simple cases of conductors, with a uniform electrical conductivity, surrounded by different solenoids. Results obtained using the model for the induction plasma are presented next. These are compared against flow, temperature, and electromagnetic fields obtained using our earlier, one-dimensional electromagnetic fields model.[1,2]

3.1. Cylindrical Load in the Infinite Solenoid

Computations were first carried out using the vector potential model for a cylindrical load of a constant electrical conductivity placed inside an infinite solenoid.[20] Figure 3 shows a comparison between the normalized magnetic field intensity profiles in the radial direction obtained using the

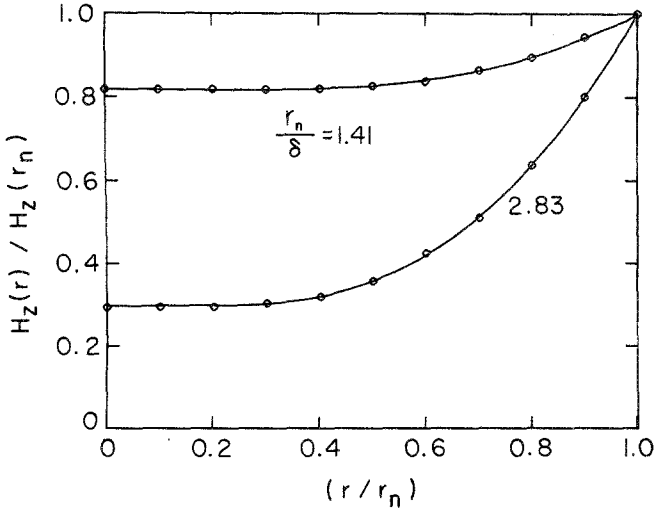

Fig. 3. Radial profiles of the axial magnetic field for a load of uniform electrical conductivity in an infinite solenoid.

present model (circles) and those of an exact solution (solid lines) for two cases, with values of $r_n/\delta = 1.41$ and 2.83, respectively. Here r_n is the radius of the cylindrical load and δ is the skin depth, defined as

$$\delta = \sqrt{2/\mu_0 \sigma \omega} \tag{39}$$

where σ is the electrical conductivity of the load. The agreement between the two results is excellent for both cases considered.

3.2. Cylindrical Load in a Short Solenoid

In contrast to the infinite solenoid case, the use of a short solenoid results in variation of the magnetic field intensity in both the radial and axial directions.

Figure 4 shows the axial magnetic field intensity profiles along the centerline of a 3-turn short solenoid, 66 mm in diameter and 40 mm long, in which a load of uniform electrical conductivity, 50 mm in diameter, is placed concentric with the solenoid. The total length of the load is assumed to be identical to that of the solenoid, i.e., 40 mm, and the electrical conductivity of the space beyond the load is assumed to be zero. Computations were carried out for different oscillator frequencies giving rise to

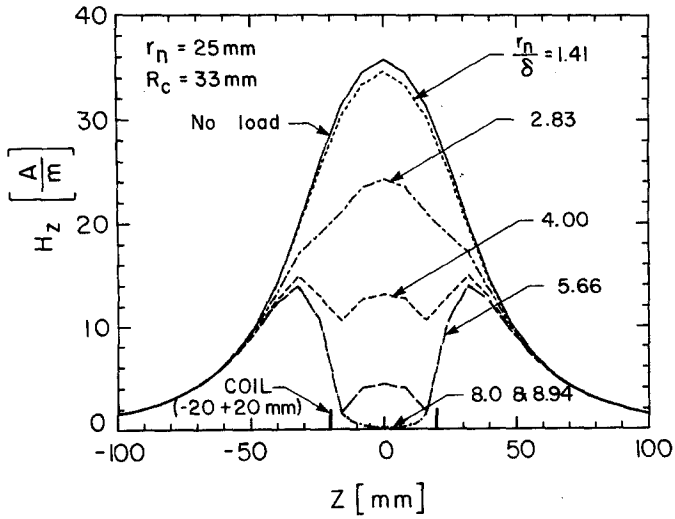

Fig. 4. Axial magnetic field distributions along the centerline of short solenoid in the absence and presence of a load of uniform electrical conductivity for various oscillator frequencies ($1.41 < r_n/\delta < 8.94$).

variations of the ratio r_n/δ between 1.41 and 8.94. The solid line on Fig. 4 corresponds to the exact solution for the case of "no-load," for comparison.

It may be noted that at low oscillator frequencies, and values of $r_n/\delta < 1.5$–2.0, the presence of the load has relatively no effect on the magnetic field distribution along the centerline of the solenoid. With the increase of the oscillator frequency, the induction currents are limited to a decreasingly small region around the outer shell of the conductor. The increase of the current density in these regions of the load results in an increase of the induced magnetic field in the center of the discharge. Since both the applied and induced magnetic fields are out of phase, the resultant magnetic field intensity along the centerline of the solenoid will drop within the load and, to a lesser extent, in the region of influence surrounding it. As shown in Fig. 4, the effect increases substantially with the decrease of the skin depth, or the increase of the r_n/δ ratio.

In most of the earlier induction plasma modelling work,[1,2] based on the one-dimensional formulation of the electromagnetic fields, it was assumed that the axial magnetic field distribution along the centerline of the coil was that of a short solenoid in vacuum. As shown in Fig. 4, this may still be considered as a reasonable approximation for plasmas generated at low oscillator frequencies, for which the value of the ratio r_n/δ is in the range of 1.4–2.0. The situation, however, is quite different at higher frequencies, for which the two-dimensional formulation of the electromagnetic fields will offer a means of taking into account the interaction between the applied and the induced magnetic fields in the coil region.

3.3. Induction Plasma Torch

In an attempt to compare the predictions of the present 2-D E&H fields model with those of our earlier model in which the E&H fields were assumed to be 1-D, computations were carried out using vector potential formulation combined with the two-dimensional continuity, momentum and energy conservation equations, and the appropriate boundary conditions, for an induction plasma torch of a standard design. Details of the torch geometry and its characteristic dimensions and operating conditions are given in Fig. 1 and Table I, respectively. The plasma gas is taken as argon at atmospheric pressure, the oscillator frequency is 3.0 MHz, and the net energy dissipated into the discharge is 5.0 kW. The equations were solved using the SIMPLER finite difference scheme[21] with a 23×35 grid network in the radial and axial directions, respectively.

Computations were also carried out for the same torch geometry and operating conditions using the earlier compute code by Mostaghimi *et al.*[1,2] based on the one-dimensional electromagnetic field formulation.

Table I. Torch Characteristic Dimensions and Operating Conditions

$r_1 = 1.70$ mm	$Q_1 = 1.0$ liter/min [Ar STP]
$r_2 = 3.70$	$Q_2 = 3.0$ liters/min [Ar STP]
$r_3 = 18.80$	$Q_3 = 21.0$ liters/min [Ar STP]
$R_0 = 25.00$	Inlet Reynolds number = 625
$R_c = 33.00$	$L_1 = 10.00$ mm
Coil = 3 turns	$L_2 = 74.00$
$d_c = 5.00$ mm	$L_T = 150.00$
$f = 3.0$ MHz	
$P_0 = 5.0$ kW	

The results for each of these two cases are presented in Fig. 5-10 in terms of the following parameters:

- Two-dimensional flow and temperature fields (Fig. 5).
- Axial profiles of the temperature and velocity fields (Fig. 6).
- Axial profiles of the magnetic field intensity along the centerline of the torch (Fig. 7).

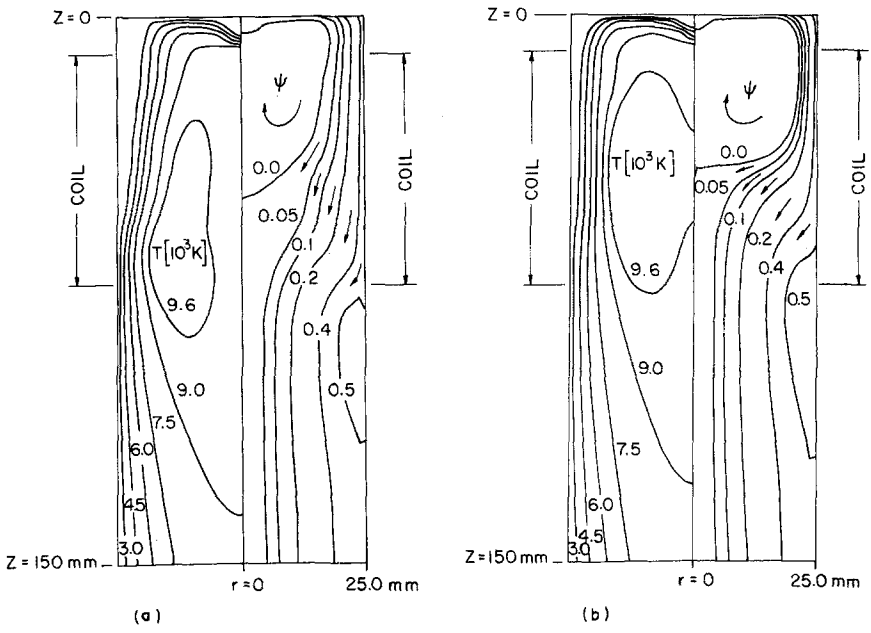

Fig. 5. Temperature and flow fields obtained using (a) the 2-D E&H field model and (b) for the 1-D case.

- Radial distributions of the magnetic and electrical fields and the phase difference between them, the electromagnetic body forces acting on the plasma, and the local energy dissipation profile at $Z = 52$ mm (Fig. 8).
- Axial distribution of the integral energy dissipation rate, and the heat flux to the wall of the plasma confinement tube (Figs. 9 and 10).

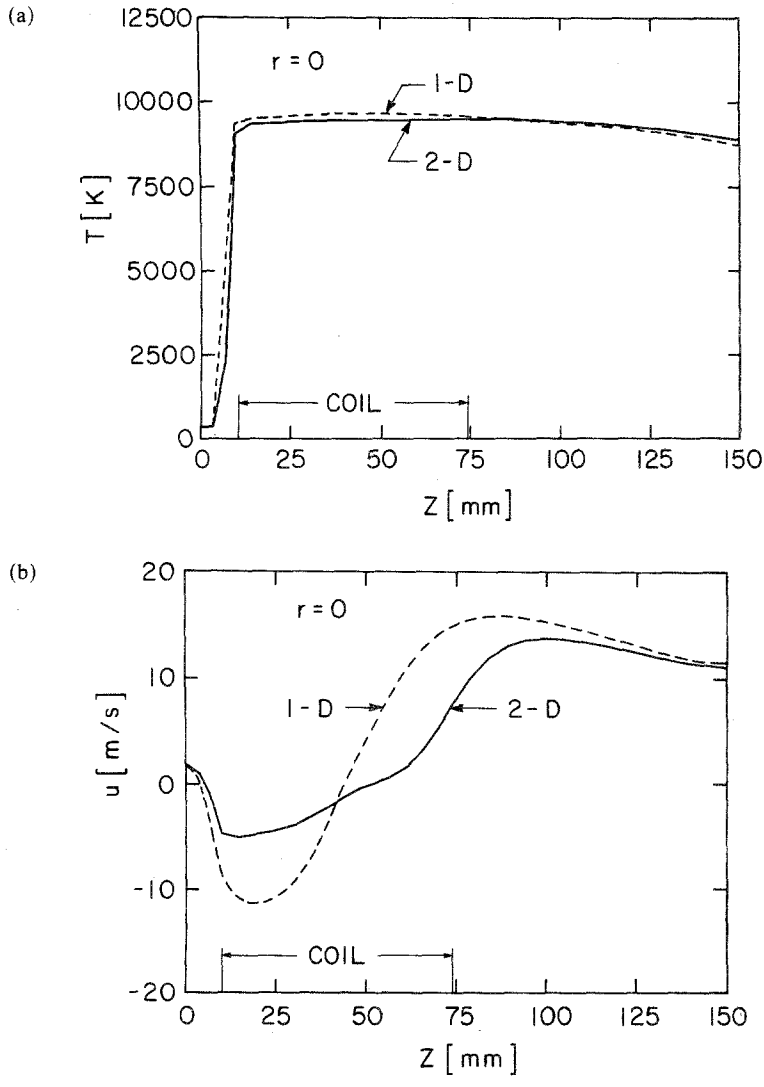

Fig. 6. Temperature (a) and velocity (b) profiles along the centerline of the plasma torch.

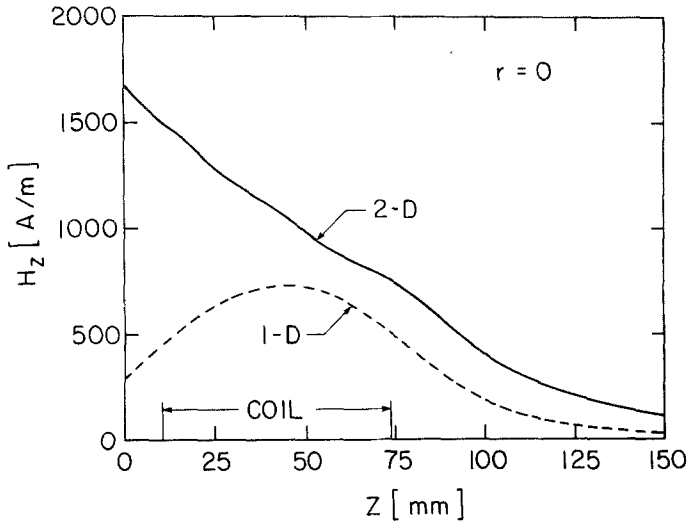

Fig. 7. Axial magnetic field distribution along the centerline of the plasma torch.

From a comparison of the isotherms and the flow streamlines given in Figs. 5a and b for the 2-D and the 1-D E&H fields models, respectively, it is noticed that while both discharge configurations have essentially similar shapes, the higher temperature region ($T > 9600$ K) is slightly shifted toward the downstream end of the coil in the 2-D case compared to that for the 1-D case. This could be partially due to the presence, for the first time, of an axial body force term, F_z, acting on the plasma. The corresponding flow fields in each case are essentially similar, giving rise to a flow separation near the wall on the downstream end of the induction coil, in addition to the characteristic recirculation eddy observed in the center of the discharge.

As shown in Fig. 6a the predicted temperature profiles along the axis of the discharge are essentially similar for the 1-D and 2-D cases studied. Figure 6b, on the other hand, shows a relatively more important effect of the electromagnetic field formulation (1-D vs. 2-D) on the axial velocity profiles along the centerline of the torch. It may be noted from Fig. 6b that the 2-D E&H field formulation gives rise to a lower backflow caused by electromagnetic pumping on the upstream end of the coil compared to that for the 1-D case.

As expected, the principal difference between the predictions of the two models is in the electromagnetic field distributions obtained (Figs. 7 and 8). It should be emphasized that in Fig. 7 the shape of the distribution

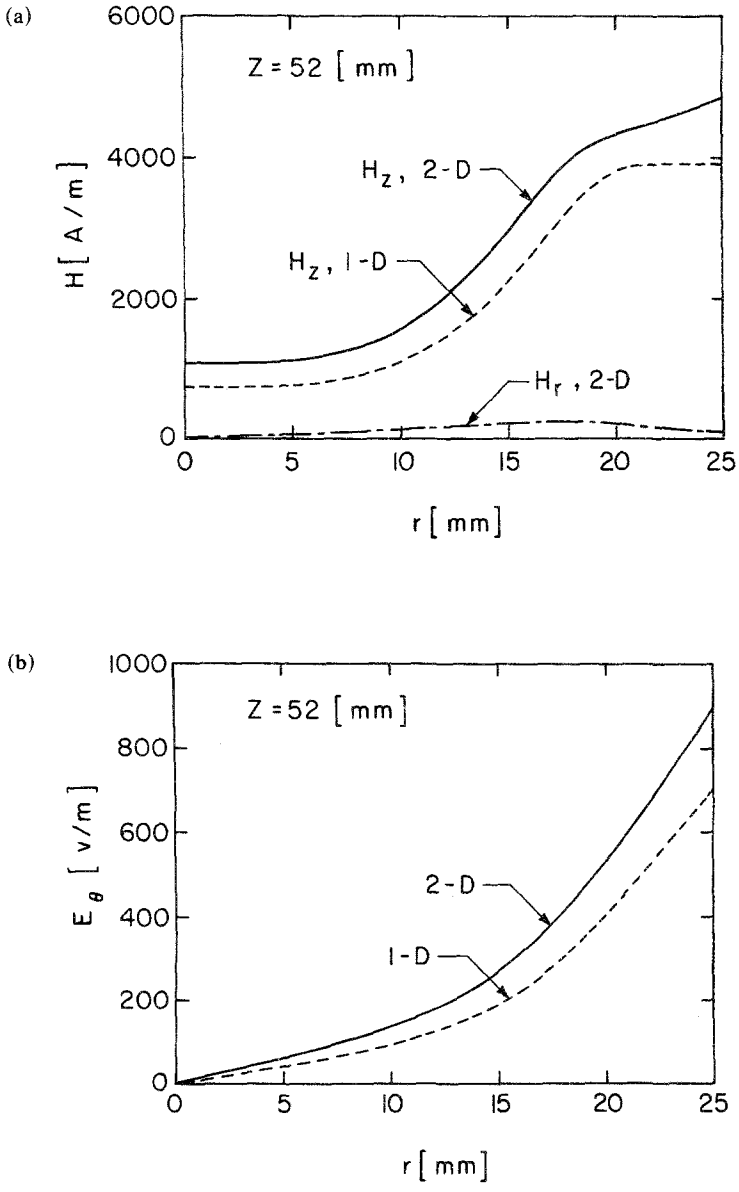

Fig. 8. Radial profiles, at $Z = 52$ mm, of the magnetic field (a), the electrical field intensity (b), the phase difference between them (c), the electromagnetic body forces acting on the plasma (d), and the local energy dissipation due to ohmic heating (e).

(c)

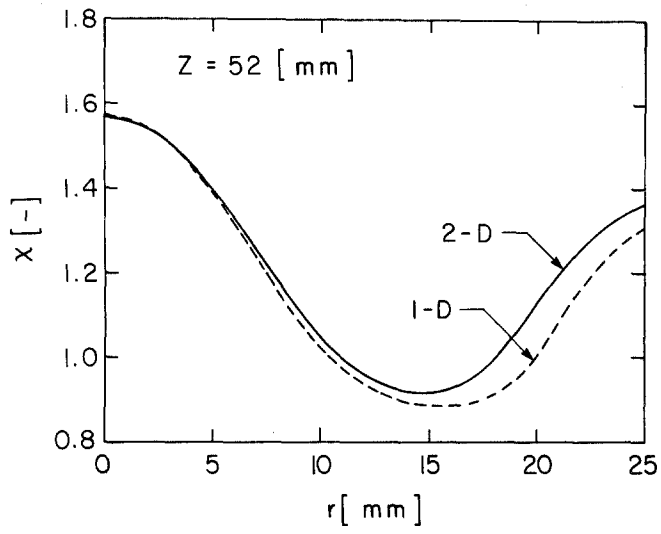

(d)

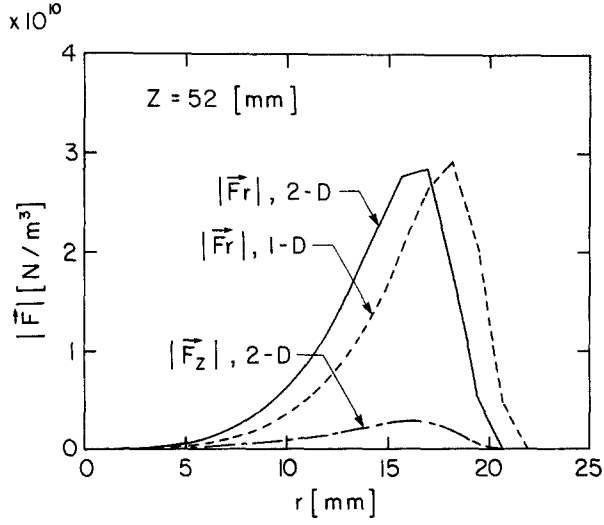

Fig. 8. Continued.

of the axial magnetic field along the centerline of the torch for the 1-D case is an imposed boundary condition which is taken as that for a short solenoid in vacuum, while the profile given for H_z in the 2-D case is one that is obtained in the course of the computation. It may be noted in the latter case that the axial magnetic field distribution is not symmetric with respect

(e)

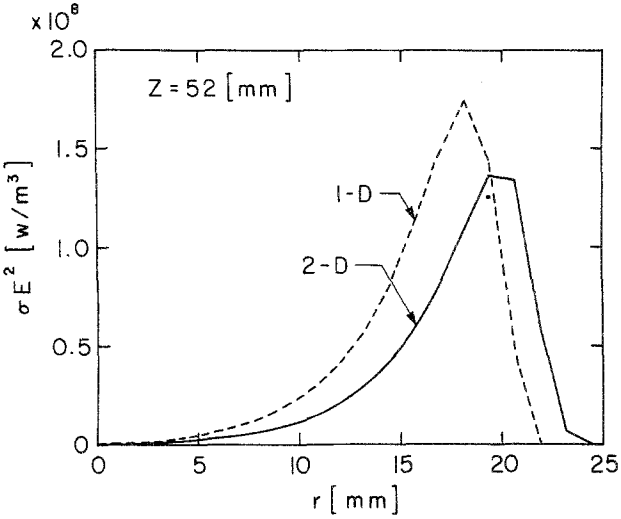

Fig. 8. Continued.

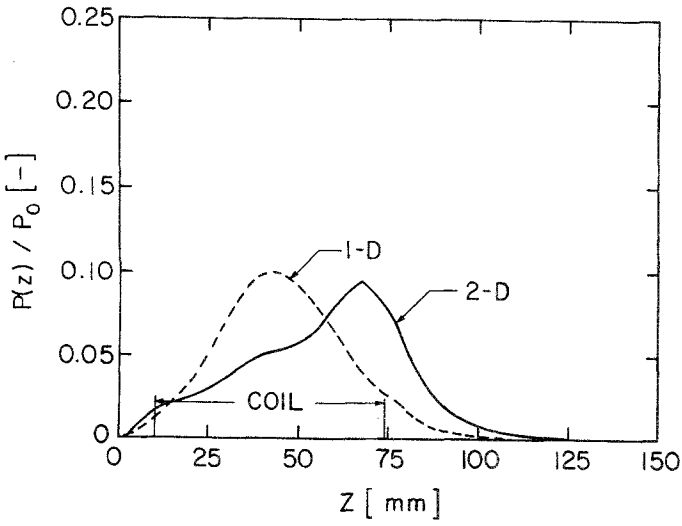

Fig. 9. Axial distributions of the integral energy dissipation in the torch.

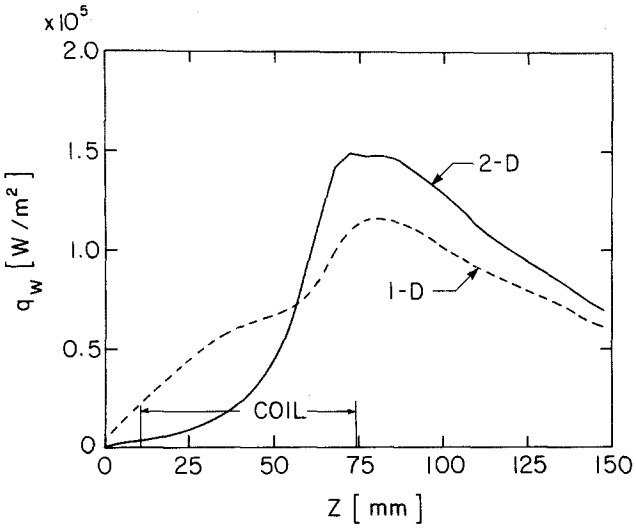

Fig. 10. Axial distributions of the heat flux to the wall of the plasma confinement tube.

to the coil and rather drops monotonously from one end of the coil to the other. The fact that the magnetic field intensity does not drop on the upstream end of the coil is, however, only a consequence of the fact that, in the torch configuration used, the induction coil is very close to the upstream end of the torch, with its first turn at only 10.0 mm from the upstream boundary of the computation space. Obviously, if the computation domain were extended further upstream, the magnetic field intensity would eventually decrease with distance from the coil.

It may be noted from Fig. 8a that while the computed radial magnetic field intensity (H_r) is considerably smaller than the axial component of the magnetic field (H_z), values of H_z obtained using the 1-D and 2-D models are substantially different. Corresponding differences, although smaller in absolute terms, are observed between the computed E_θ and χ fields in each case, as shown in Figs. 8b and 8c.

Figures 8d and 8c show, respectively, the corresponding radial distributions of the body forces $|\mathbf{F}|$ and the local energy dissipation σE^2. The 2-D model gives rise to body forces in the radial, F_r, and axial, F_z, directions in contrast to the 1-D model which, by definition, can account for the radial body forces only. Corresponding differences are noted in the local energy distribution profiles. These are responsible for the modification of the axial distributions of the integral energy dissipation in the torch and of the heat flux to the wall of the plasma confinement tube as shown in Figs. 9 and 10 respectively.

4. CONCLUSIONS

A two-dimensional representation of the electromagnetic fields in an inductively coupled r.f. plasma is presented using the vector potential approach. Computations carried out for a short coil in which a cylindrical load of uniform electrical conductivity is placed show an important effect of the operating frequency, or the ratio r_n/δ, on the resultant magnetic field distribution in the coil region. The magnetic field along the centerline of the coil approaches that of a short solenoid in vacuum for a value of r_n/δ lower than 1.5.

For an induction plasma under typical operating conditions, some differences are noted between the flow and electromagnetic fields predicted by the two-dimensional model compared to those obtained using the earlier one-dimensional model. The significance of the present model is, however, in its ability to predict the effects of the coil geometry on the flow and temperature fields in the discharge. It also provides a more realistic representation of the electromagnetic fields in the coil region which can have an important influence on the energy distribution in the plasma specially under high-frequency operating conditions.

ACKNOWLEDGMENT

This work has been carried out in a collaborative effort with Drs. Pengyuan Yang and Ramon M. Barnes of the Department of Chemistry, University of Massachusetts, Amherst, Massachusetts. The financial support by the Ministry of Education of the Province of Québec and the Natural Sciences and Engineering Research Council of Canada is gratefully acknowledged.

REFERENCES

1. J. Mostaghimi, P. Proulx, and M. Boulos, *Numer. Heat Transfer* **8**, 187 (1985).
2. J. Mostaghimi, P. Proulx, and M. Boulos, *Plasma Chem. Plasma Process.* **4**, 199 (1984).
3. T. Yoshida, K. Nakagawa, T. Harada, and K. Akashi, *Plasma Chem. Plasma Process.* **1**, 113 (1981).
4. P. Proulx, J. Mostaghimi, and M. I. Boulos, *Int. J. Heat Mass Transfer* **28**, 1327 (1985).
5. P. Proulx, J. Mostaghimi, and M. I. Boulos, *Plasma Chem. Plasma Process.* **7**, 29 (1987).
6. J. Mostaghimi, P. Proulx, and M. I. Boulos, *Spectrochimica Acta B* **40**, 153 (1985).
7. J. Mostaghimi, P. Proulx, and M. I. Boulos, *J. Appl. Phys.* **61**, 1753 (1987).
8. M. I. Boulos, *Pure Appl. Chem.* **57**, 1321 (1985).
9. M. I. Boulos and R. M. Barnes, "Plasma Modelling and Computer Simulation," in *Inductively Coupled Plasma Emission Spectroscopy*, Wiley, New York (1987), Chapter 9, p. 289.

10. S. V. Dresvin, ed., *Physics and Technology of Low-Temperature Plasmas*, Iowa State University Press, Ames, Iowa (1977), pp. 329–350.
11. M. Mitchner and C. H. Kruger, Jr., *Partially Ionized Gases*, Wiley, New York (1973).
12. J. D. Jackson, *Classical Electrodynamics*, Wiley, New York (1962); Part II, P. W. J. M. Boumans, ed., Wiley, New York (1987).
13. J. W. McKelliget, "A Mathematical Model of an Inductively Coupled Plasma Torch," University of Lowell, Internal Report, TR86-112.1 (1986).
14. J. W. McKelliget and N. El-Kaddah, "Theoretical Prediction of the Effect of Coil Configuration on the Gas Mixing in an Inductively Coupled Plasma," MRS Symposium on Plasma Processing and Synthesis of Materials, Anaheim, California (1987).
15. J. Mostaghimi, "Two-Dimensional Electromagnetic Fields in R.F. Inductively Coupled Plasmas," University of Sherbrooke, Internal Report (1987).
16. G. A. Korn and T. M. Korn, *Mathematical Handbook for Scientists and Engineers*, 2nd ed., McGraw-Hill, New York (1968).
17. J. L. Lewis, "The Motion of Particles Entrained in a Plasma Jet," Ph.D. Thesis, McGill University (1971).
18. D. L. Evans and R. S. Tankin, *Phys. Fluids* **10**, 1137–1144 (1967).
19. R. S. Devoto, *Phys. Fluids* **9**, 1230–1240 (1966).
20. A. E. Mensing and L. R. Boedecker, NASA Contract Report CR-1312 (1969).
21. S. V. Patankar, *Computational Fluid Flow and Heat Transfer*, McGraw-Hill, New York (1980).